Device Benchmark Comparisons via Kinetic, Hydrodynamic, and High-Field Models

Carlo Cercignani[*], Irene M. Gamba[†], Joseph W. Jerome[‡], and Chi-Wang Shu[§]

Abstract

This paper describes benchmark comparisons for a GaAs $n^+ - n - n^+$ diode. A global kinetic model is simulated, and compared with various realizations of the hydrodynamic model, depending on mobility calibration. Finally, the channel region alone is simulated, with interior boundary conditions derived from the kinetic model, by use of the high-field (augmented drift-diffusion) model.

Keywords: Kinetic model, hydrodynamic model, augmented drift-diffusion, high-field model, domain decomposition

Acknowledgments: The first author is supported by M.U.R.S.T. of Italy. The second author is supported by the National Science Foundation under grant DMS-9623037. The third author is supported by the National Science Foundation under grants DMS-9424464 and DMS-9704458. The fourth author is supported by the National Science Foundation under grant ECS-9627849 and the Army Research Office under grant DAAG55-97-1-0318.

[*]Politecnico di Milano, 20133 Milano, Italy.
tel: 0039-2-23994557, Fax: 0039-2-23994568, email: carcer@mate.polimi.it

[†]Department of Mathematics and Texas Institute of Computational and Applied Mathematics, University of Texas, Austin, TX 78712.
tel: (512) 471-7150, Fax: (512) 471-9038, email: gamba@math.utexas.edu

[‡]Department of Mathematics, Northwestern University, Evanston, IL 60208.
tel: (847) 491-5575, Fax: (847) 491-8906, email: jwj@math.nwu.edu; corresponding author.

[§]Division of Applied Mathematics, Brown University, Providence, RI 02912.
tel: (401) 863-2549, Fax: (401) 863-1355, email: shu@cfm.brown.edu

1 Introduction

In previous work [3], the authors introduced a conceptual domain decomposition approach, combining drift-diffusion, kinetic, and high-field regimes. The high-field model had been introduced in [5]. The approach was implemented in preliminary form in [4]. More precisely, the hydrodynamic model was used as a global calibrator (see also [8, 9]), and used to define internal boundary conditions, separating drift-diffusion from high-field regions. In particular, it was found that this methodology allowed for a validation of the high-field model in the channel region. In this paper, we continue the program begun in [3]. We again define a global calibrator, a linear approximation to the Boltzmann transport equation, and solve this in one space and one velocity dimension. In the process, we compare this global calibrator with the hydrodynamic model, and explore the role of mobility coefficients in the matching. The role of the latter had been carefully explored in [8]. The direct comparison of the kinetic and hydrodynamic models underscores how significantly the mobility expressions (scaled relaxation) affect the performance characteristics as predicted by the hydrodynamic model.

Secondly, we test the high-field model against the kinetic model in the channel region, where it is known that the asymptotic assumptions used to derive the high-field model are satisfied. We see the effectiveness of the high-field model, a form of augmented drift-diffusion, as compared to drift-diffusion itself. It is our hope that we shall develop an effective domain decomposition method, modeled by a combination of drift-diffusion, kinetic, and high field models in appropriate regions.

In order to provide a succinct summary of our objectives, we have carried out a detailed study of multiscale parameters and domain decomposition for the scales corresponding to the low density approximation for a GaAs channel under strong relative field, with the ultimate purpose of speeding up kinetic computations.

2 Models Employed in This Paper

The following models are used in this paper.

2.1 The Kinetic Model

The one-dimensional kinetic model can be written as follows:

$$\frac{\partial f(x,u,t)}{\partial t} + u\frac{\partial f(x,u,t)}{\partial x} - \frac{e}{m}E(x,t)\frac{\partial f(x,u,t)}{\partial u} = \frac{n(x,t)M(u) - f(x,u,t)}{\tau}, \tag{2.1}$$

where f is the scaled probability density function, x is the spatial variable, t is the time variable, u is the velocity in phase space, m is the effective electron mass, e is the electron charge unit, and

$$M(u) = \frac{1}{\sqrt{2\pi\theta}}e^{-\frac{u^2}{2\theta}} \tag{2.2}$$

is a Maxwellian, with

$$\theta = \frac{k_b}{m}T_0, \tag{2.3}$$

where k_b is the Boltzmann constant and T_0 is the lattice temperature. The concentration $n(x,t)$ is obtained by

$$n(x,t) = \int_{-\infty}^{\infty} f(x,u,t)du. \tag{2.4}$$

Also, the electric field $E(x,t)$ is obtained by solving the coupled potential equation,

$$E(x,t) = -\phi_x, \qquad (\epsilon\phi_x)_x = e(n - n_d), \tag{2.5}$$

with the boundary conditions

$$\phi(0,t) = 0, \qquad \phi(0.8,t) = vbias, \tag{2.6}$$

where ϵ is the dialetric constant, n_d is the doping, $vbias$ is the voltage bias, and the relaxation parameter τ is computed by

$$\tau = \frac{m\mu}{e}. \tag{2.7}$$

Here μ is the mobility and we have examined the following different characterizations.

1. Constant μ. We have used values:

$$\mu = 0.75\,\mu m^2/(V\,ps) \text{ (see [2])}. \tag{2.8}$$

$$\mu = 4.0\,\mu m^2/(V\,ps) \text{ (channel value extrapolation)}. \tag{2.9}$$

2. Variable μ depending on the doping n_d:

$$\mu = \begin{cases} 0.75\,\mu m^2/(V\,ps), & \text{in the } n^+ \text{ region } n_d = 10^6 \mu m^{-3}, \\ 4.0\,\mu m^2/(V\,ps), & \text{in the } n^- \text{ region } n_d = 2 \times 10^3 \mu m^{-3}. \end{cases} \tag{2.10}$$

   This formula is a modified Caughey-Thomas model [6] and reflects the fact that mobility is larger in lightly doped regions and smaller in heavily doped regions.

3. Variable μ depending on the electric field E, used in drift-diffusion simulations to model saturation (see [7]):

$$\mu(E) = 2\mu_0 / \left[1 + \sqrt{1 + 4(\mu_0 |E|/v_d)^2}\right], \tag{2.11}$$

   where

$$\mu_0 = 4.0\ \mu m^2/(V\,ps), \qquad v_d = 2.0\ \mu m/ps. \tag{2.12}$$

   v_d here is taken to be the maximum of the velocity in the kinetic run with $vbias = 1.0$ and $\mu = 4$.

The kinetic model (2.1) is chosen because of its mathematical simplicity and should certainly be modified in future work on the method. The main drawback of the collision term is that all the moments except that of zeroth order (which is conserved by collisions) relax to their equilibrium values at the same rate. Now momentum and energy (which are the most important among these moments) certainly relax at rather different rates, especially because of the small value of the (effective) mass of the electrons, which implies a non-negligible amount of elastic scattering.

2.2 The Hydrodynamic (HD) Model.

The system assumes the form defined by conservation of particle number n, momentum p, and energy w. It is derived in [7].

Conservation of Particle Number

$$n_t + (nv)_x = 0, \tag{2.13}$$

Conservation of Momentum

$$p_t + (pv + nk_bT)_x = enE - (p/\tau_p), \tag{2.14}$$

Conservation of Energy

$$w_t + (vw + nvkT)_x = envE - \frac{w - w_0}{\tau_w} + (\kappa nT_x)_x, \tag{2.15}$$

where $v = \frac{p}{mn}$ is the velocity, T is the temperature, κ is the thermal conductivity coefficient governed by the Wiedemann-Franz law, $w_0 = \frac{3}{2}nk_bT_0$ denotes the rest energy. These equations are coupled to the electrostatic equation (2.5) defining E. The expressions τ_p and τ_w are standard momentum and energy relaxation expressions (see [1]).

2.3 The Drift-Diffusion (DD) Model.

The drift-diffusion (DD) model is well documented (see, for example, [7]). It is given by:

$$n_t + J_x = 0, \tag{2.16}$$

where

$$J = J_{hyp} + J_{vis},$$

and

$$J_{hyp} = -\mu nE,$$

$$J_{vis} = -\tau(n\theta)_x.$$

2.4 The High-Field (HF) Model.

The model can be written as follows:

$$n_t + J_x = 0, \tag{2.17}$$

where

$$J = J_{hyp} + J_{vis},$$

and

$$J_{hyp} = -\mu n E + \tau\mu \left(\frac{e}{\epsilon}\right) n(-\mu n E + \omega),$$

$$J_{vis} = -\tau[n(\theta + 2\mu^2 E^2)]_x + \tau\mu E(\mu n E)_x.$$

For our current one dimensional case, ω is taken to be a constant:

$$\omega = (\mu n E)|_{x=0}.$$

It is developed in [5] by asymptotic expansion methods (Chapman-Enskog) for the kinetic formulation of the problem (2.1)–(2.5), under strong forcing scaling assumptions.

Other augmented drift-diffusion models are found in [13, 11]. The development of [5] requires three dimensionless parameters, viz. ,

- The ratio η of drift and free velocity (the latter usually taking on the thermal velocity):

$$\eta = U/\bar{\theta}^{1/2}, \tag{2.18}$$

  where U, in units of velocity, is given by

$$\frac{\tau e}{m}\frac{[\phi]}{L},$$

  for a length scale L and a potential drop $[\phi]$;

- The scaled mean free path ε:

$$\varepsilon = \frac{\tau\bar{\theta}^{1/2}}{L}; \tag{2.19}$$

- The scaled Debye length γ from the electrostatic potential equation of a self-consistent model:

$$\gamma = \frac{\bar{\rho} e L^2}{\epsilon[\phi]}, \tag{2.20}$$

where $\bar{\rho}$ scales the density of the fixed background $n_d(x)$.

For η of the same order of ε and both very small as in the highly doped regions, the Chapman-Enskog expansion associated with system (2.1)-(2.5) yields the DD equations (2.16). However, inside the channel region, η becomes of order of one as well as γ. Here the corresponding expansion yields the high-field model (2.17).

3 Channel Simulation

The device we consider for this paper is the one dimensional GaAs n^+-n-n^+ structure of length $0.8\mu m$. The device used is as follows: $x \in [0, 0.8]$; the doping is defined by $n_d(x) = 10^6/\mu m^3$ in $0 \leq x \leq 0.175$ and in $0.625 \leq x \leq 0.8$, and by $n_d(x) = 2 \times 10^3/\mu m^3$ in $0.225 \leq x \leq 0.575$, with a smooth intermediate transition. Notice our choice of units: this is exactly the device used in Baranger and Wilkins [2], with $n_d(x) = 10^{18}/cm^3$ in the high doping region and $n_d(x) = 2 \times 10^{15}/cm^3$ in the low doping region, except for a smooth transition of width $0.05\mu m$ at the junctions.

More specific conditions for various models are listed below.

1. For the kinetic model (2.1):

   - The velocity space is artificially cut at

$$-a \leq u \leq a \tag{3.1}$$

where we monitor to ensure that $f(x, u, t)$ is always very small at the boundary $u = \pm a$ for the final steady state results. We learned that it is more than enough

in all our runs to use $a = 3.5$. Larger values of a are also used to verify that graphical results do not change.

- We use a uniform grid both in x and in u, with 160×150 points. A more refined mesh is also used to verify that the results do not change in the pictures.
- At $x = 0$, take

$$f(0, u, t) \;=\; n_d(0)\, M(u) \tag{3.2}$$

if $u \geq 0$, and no boundary condition (extrapolation of the numerical solution from inside the domain to the boundary) if $u < 0$. Also take $\phi(0, t) = 0$.

- At $x = 0.8$, take

$$f(0.8, u, t) \;=\; n_d(0.8)\, M(u) \tag{3.3}$$

if $u \leq 0$, and no boundary condition (extrapolation of the numerical solution from inside the domain to the boundary) if $u > 0$. Also take $\phi(0.8, t) = vbias$.

- At $u = -a$ and $u = a$, take no boundary condition (extrapolation of the numerical solution from inside the domain to the boundary).

2. For the hydrodynamic (HD) model (2.13)-(2.15):

- We use a uniform grid in x with 160 points.
- At $x = 0$, take

$$n(0, t) = n_d(0), \qquad T(0, t) = T_0, \qquad \phi(0, t) = 0, \tag{3.4}$$

with other quantities extrapolated from inside the computational domain to the boundary.

- At $x = 0.8$, take

$$n(0.8, t) = n_d(0.8), \qquad T(0.8, t) = T_0, \qquad \phi(0.8, t) = vbias, \tag{3.5}$$

with other quantities extrapolated from inside the computational domain to the boundary.

3. For both the drift-diffusion (DD) model (2.16) and the high-field (HF) model (2.17) applied in the middle region [0.25, 0.55]:

   - We use a uniform grid in x with 100 points.
   - At the boundaries $x = 0.25$ and $x = 0.55$, n and ϕ take the boundary values obtained from the global kinetic simulation results evaluated at $x = 0.25$ and $x = 0.55$.

Simulations are performed for *vbias* from 0V to 2V, and results are shown for selected cases to save space. Other parameters: $m = 0.065 \times 0.9109$ $(10^{-30}Kg)$, $e = 0.1602$ $(10^{-18}C)$, $k_b = 0.138046 \times 10^{-4}$ $(10^{-18}J/Kelvin)$, $\epsilon = 13.2 \times 8.85418$ $(10^{-18}F/\mu m)$.

4 Numerical Algorithm

We use the ENO schemes developed in [12] and the weighted ENO (WENO) schemes developed in [10]. ENO and WENO schemes are designed for hyperbolic conservation laws or other problems containing either discontinuous solutions or solutions with sharp gradients. The guiding principle is an adaptive local choice of a stencil (ENO), or use of a nonlinear convex combination of contributions from local stencils (WENO), so that contributions from stencils containing a possible discontinuity or other unpleasant features (e.g., a high gradient) are either completely avoided (ENO) or are assigned a nearly zero weight (WENO). In doing this, uniform high order accuracy can be achieved without introducing any oscillations near discontinuities or sharp gradient regions. We use the third order ENO schemes [12] for the hydrodynamic model simulation, and the fifth order WENO schemes [10] for all other models in this paper. The high order accuracy of these algorithms allows us to use relatively coarse grids and still get very accurate results. The algorithms are extremely stable and robust in all the numerical simulations. In order to verify the stability and robustness of the numerical algorithm, we have also simulated the kinetic and hydrodynamic models to a

higher doping $vbias = 3$ and for a smaller device (of length $0.4\mu m$). The numerical solution converges without any problem. The results are not shown here.

5 Simulation Results

In all the numerical simulations, we perform a long time integration until a steady state is reached.

In Fig. 5.1, Fig. 5.2 and Fig. 5.3 we show the results of the kinetic simulation for $vbias = 1$ volt with various forms of mobility μ, given by (2.8), (2.9), (2.10) and (2.11). Fig. 5.1 contains the results of concentration n, velocity v

$$v(x,t) \;=\; \int_{-\infty}^{\infty} uf(x,u,t)du \,/\, n(x,t), \tag{5.1}$$

electric field E and potential ϕ. Fig. 5.2 contains the results of the I-V curve with

$$I \;=\; \frac{e}{b-a}\int_a^b n(x,t)v(x,t)dx. \tag{5.2}$$

Notice that the collision integrals conserve particle number, hence $n(x,t)v(x,t)$ should be a constant in steady states. We still take the average in (5.2) in the whole region $[a,b]$=[0, 0.8] to compute I. The quantity η, defined in (2.18), which is useful for the verification of suitability for the high-field model (see Section 2.4), is also plotted in Fig. 5.2. Fig. 5.3 contains the probability density function $f(x,u,t)/n(x,t)$ at $x = 0.2$ and $x = 0.5$.

For this channel, the scaled mean free path ε defined in (2.19) is in the range of 0.18 to 0.98, depending on the mobility assumptions, and the scaled Debye length γ defined in (2.20) is in the range of 10000 to 20000 inside the channel but very large near the boundaries.

From Fig. 5.1, Fig. 5.2 and Fig. 5.3 we can see that different mobility assumptions yield significantly different results, especially in velocity, and hence also affect the I-V curves. This indicates that, when using kinetic results as benchmarks, one must be careful regarding the mobility assumptions. In particular, the results of $\mu = 4$ and $\mu = \mu(n_d)$ as given by

(2.10) produce almost identical results, but these results are significantly different from those obtained by $\mu = 0.75$ and by $\mu = \mu(E)$ as given by (2.11).

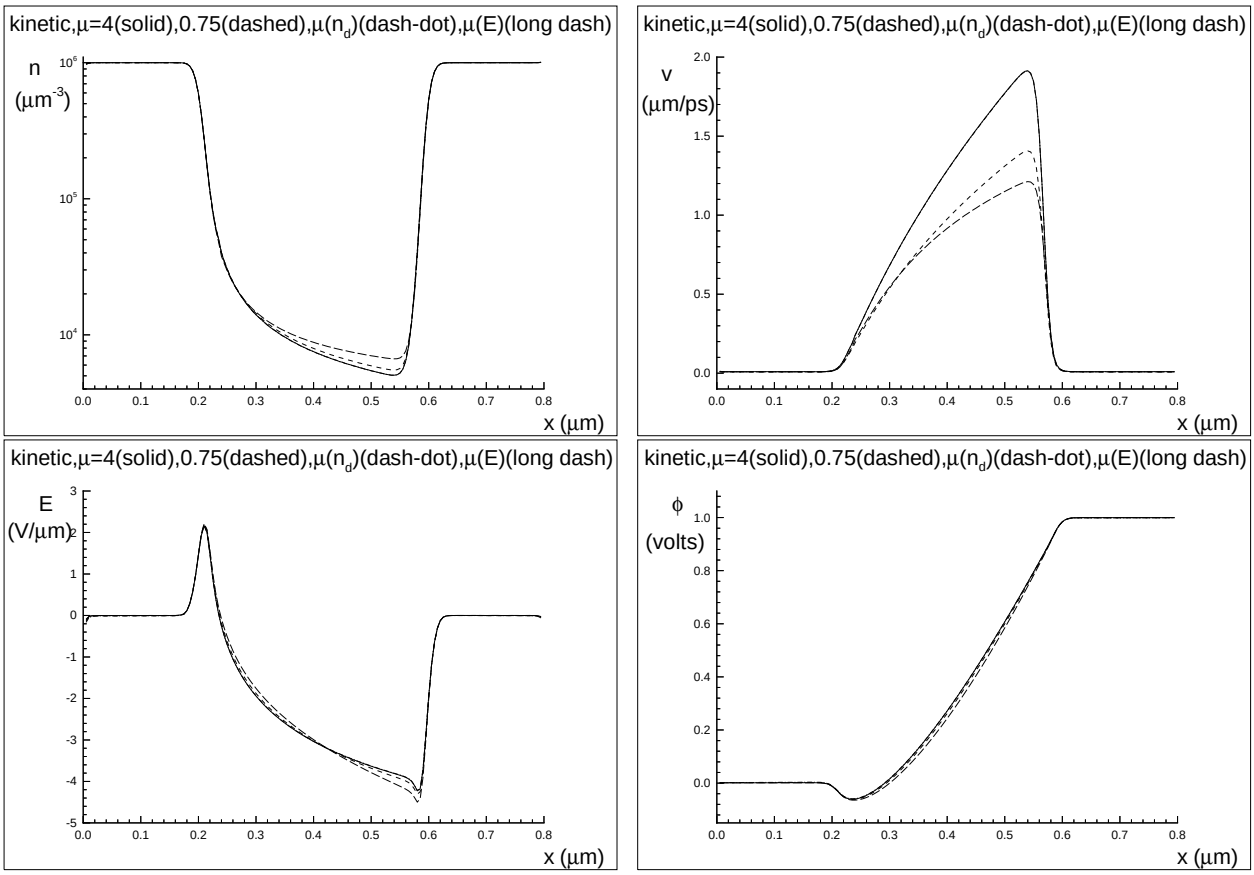

Figure 5.1: Kinetic simulation results of $vbias = 1$ volt with various assumptions on μ. Solid line: $\mu = 4$; dashed line: $\mu = 0.75$; dash-dot line: $\mu = \mu(n_d)$ as given by (2.10); long dashed line: $\mu = \mu(E)$ as given by (2.11). Top left: the concentration n in μm^{-3}; top right: the velocity v in $\mu m/ps$; bottom left: the electric field E in $volts/\mu m$, bottom right: the potential ϕ in $volts$.

We then compare the simulation results of the hydrodynamic (HD) model, defined in Section 2.2, with various assumptions on μ as given in (2.8), (2.9), (2.10) and (2.11), with the kinetic simulation results obtained with the same mobility assumptions. Fig. 5.4 shows the results of concentration n, Fig. 5.5 shows the results of velocity v, Fig. 5.6 gives the results of electric field E, and Fig. 5.7 shows the I-V curves. We can see that the comparison results between the two models are very similar for $\mu = 4$ and $\mu = \mu(n_d)$ as given by (2.10), but are quite different (especially in velocity and the I-V curve) for $\mu = 0.75$ and $\mu = \mu(E)$. For

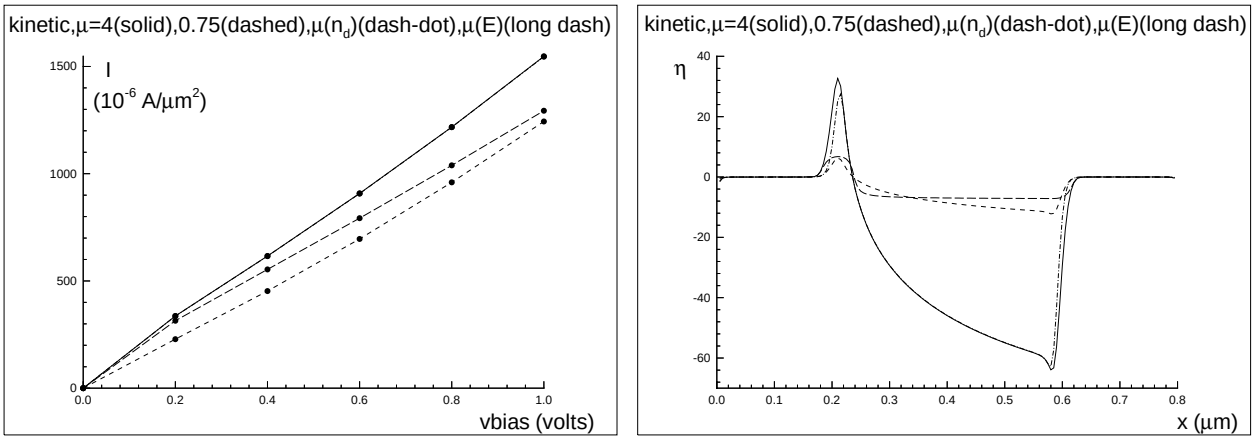

Figure 5.2: Kinetic simulation results with various assumptions on μ. Solid line: $\mu = 4$; dashed line: $\mu = 0.75$; dash-dot line: $\mu = \mu(n_d)$ as given by (2.10); long dashed line: $\mu = \mu(E)$ as given by (2.11). Left: the I-V curve in $10^{-6} Amps/\mu m^2$ versus $volts$; right: the quantity η defined in (2.18) at $vbias = 1$ volt.

the hydrodynamic model, the average in (5.2) to obtain the current I is taken in the middle region $[a, b]$=[0.3, 0.5] where numerical fluctuation is the smallest.

Guided by the value of η in Fig. 5.2, we perform a preliminary domain decomposition experiment, in the middle region [0.25,0.55] where η is large in magnitude, using the drift-diffusion (DD) model and the high-field (HF) model, with boundary conditions for n and ϕ provided by the global kinetic simulations. The mobility model for both the DD and HF simulations is taken as $\mu = \mu(E)$ given by (2.11). This seems to be the only mobility assumption which will cause the DD or HF results to be close to those of the kinetic simulations. In [4] we have performed a similar study for a slightly different channel, using boundary conditions provided by the hydrodynamic (HD) simulations.

In Fig. 5.8 we plot the comparison among the mid-region simulations of DD and HF, and the global kinetic simulation, for the quantities n and E, at $vbias = 1$V. We perform the mid-region simulation for HF and DD both with the boundary conditions provided by the kinetic simulation using $\mu = 4$ (bottom in Fig. 5.8), and with the boundary conditions provided by the kinetic simulation using $\mu = \mu(E)$ given by (2.11) (top in Fig. 5.8). We can see that the high-field model has a much better agreement with the kinetic simulations. In

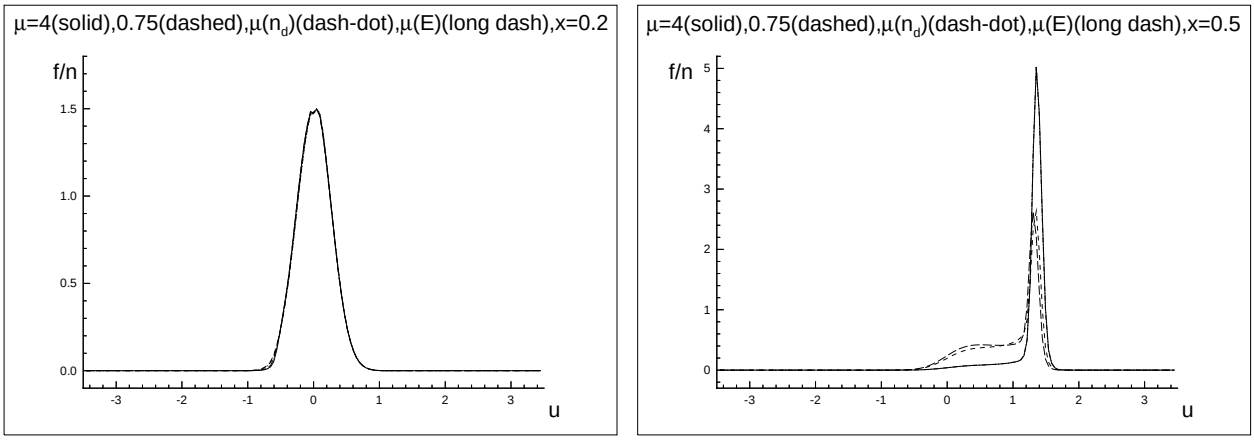

Figure 5.3: The probability density function $f(x,u,t)/n(x,t)$ of the kinetic simulation with various assumptions on μ. Solid line: $\mu = 4$; dashed line: $\mu = 0.75$; dash-dot line: $\mu = \mu(n_d)$ as given by (2.10); long dashed line: $\mu = \mu(E)$ as given by (2.11). Left: at $x = 0.2\mu m$; right: at $x = 0.5\mu m$.

Fig. 5.9 we plot the I-V curve. The current I is obtained by

$$I = \frac{e}{b-a}\int_a^b J(x,t)dx \tag{5.3}$$

with $J(x,t)$ given by (2.16) or (2.17), respectively. The average in (5.3) is taken in the middle region $[a,b]$=[0.3, 0.5] where numerical fluctuation is the smallest. Clearly the HF model is in better agreement with the kinetic results at least for *vbias* large enough (approximately 1.5V to 2V). However, notice that even when $vbias = 1$V where the I-V characteristic of the HF is in poor agreement with the kinetic results, the agreement for the concentration n and the electric field E is already excellent, Fig. 5.8.

References

[1] G. Baccarani and M.R. Wordeman. An investigation of steady-state velocity overshoot effects in Si and GaAs devices. *Solid State Electr.*, **28**:407–416, 1985.

[2] H. U. Barenger and J. W. Wilkins, Ballistic structure in the electron distribution function of small semiconducting structures: General features and specific trends. *Phys. Rev. B*, **36**:1487–1502, 1987.

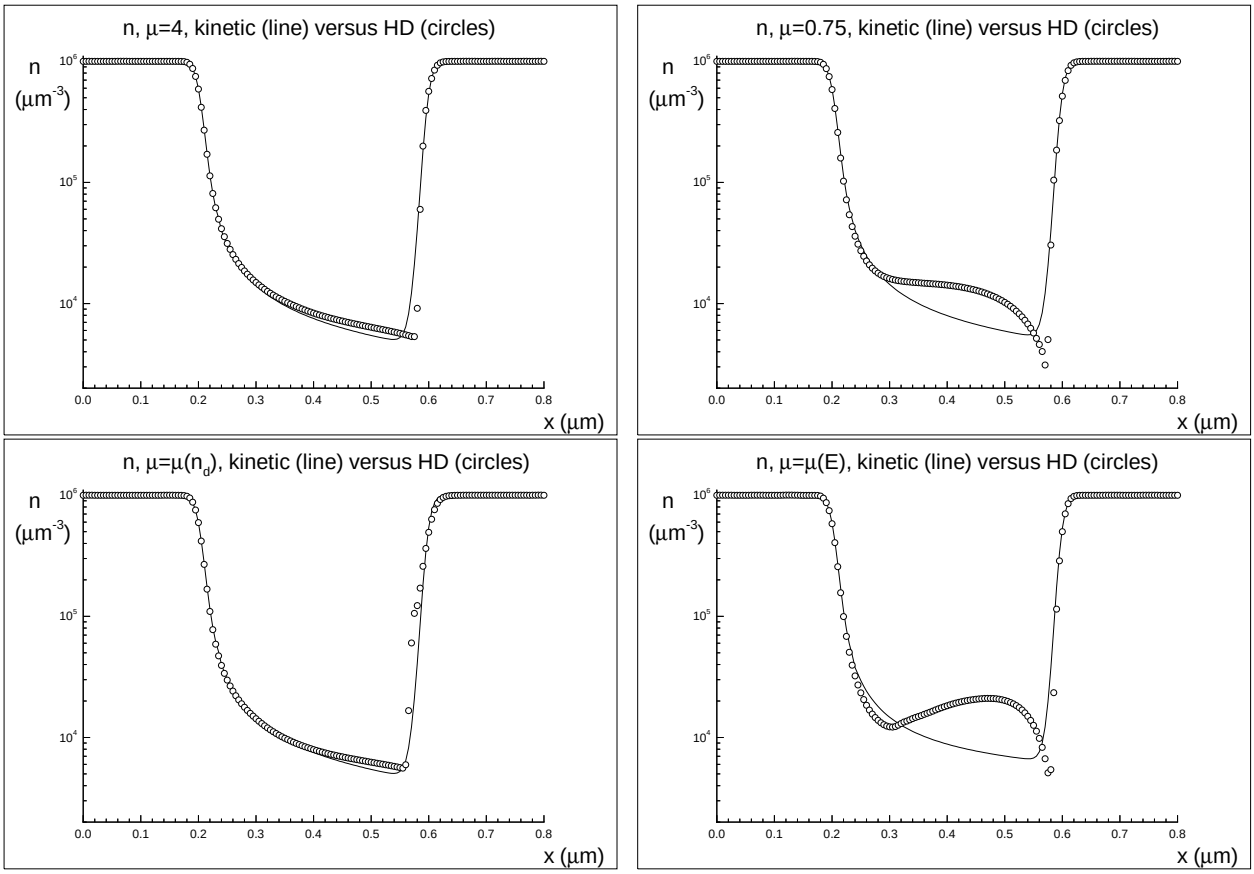

Figure 5.4: Hydrodynamic (HD) results (circles) versus kinetic simulation results (solid line), $vbias = 1$ volt. The concentration n in μm^{-3}. Top left: $\mu = 4$; top right: $\mu = 0.75$; bottom left: $\mu = \mu(n_d)$ as given by (2.10); bottom right: $\mu = \mu(E)$ as given by (2.11).

[3] C. Cercignani, I. M. Gamba, J. W. Jerome and C-W. Shu. Applicability of the high-field model: An analytical study based on asymptotic parameters defining domain decomposition. *VLSI DESIGN*, **8**:135–141, 1998.

[4] C. Cercignani, I. M. Gamba, J. W. Jerome and C-W. Shu. Applicability of the high-field model: A preliminary numerical study. *VLSI DESIGN*, **8**:275–282, 1998.

[5] C. Cercignani, I. M. Gamba and C. D. Levermore. High field approximations to Boltzmann-Poisson system boundary conditions in a semiconductor. *Appl. Math. Lett.*, **10**:111–117, 1997.

[6] D. Chen, E. C. Kan, U. Ravaioli, C. W. Shu and R. W. Dutton, An improved energy

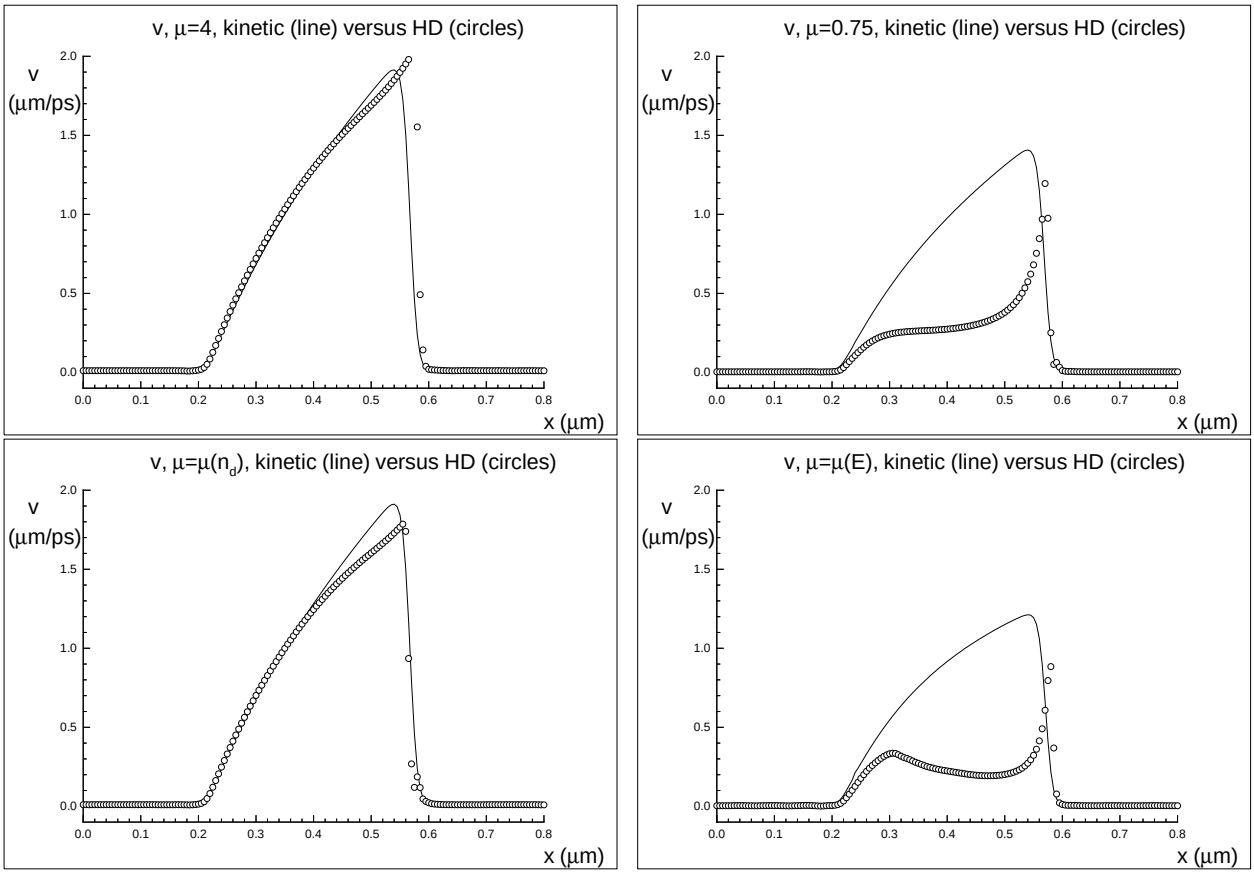

Figure 5.5: Hydrodynamic (HD) results (circles) versus kinetic simulation results (solid line), $vbias = 1$ volt. The velocity v in $\mu m/ps$. Top left: $\mu = 4$; top right: $\mu = 0.75$; bottom left: $\mu = \mu(n_d)$ as given by (2.10); bottom right: $\mu = \mu(E)$ as given by (2.11).

transport model including nonparabolicity and non-Maxwellian distribution effects. *IEEE Electron Device Letters*, **13**:26–28, 1992.

[7] J. W. Jerome. *Analysis of Charge Transport; A Mathematical Study of Semiconductor Devices*. Springer, 1996.

[8] J. W. Jerome and C.-W. Shu. The response of the hydrodynamic model to heat conduction, mobility, and relaxation expressions. *VLSI DESIGN*, **3**:131–143, 1995.

[9] J. W. Jerome and C.-W. Shu. Transport effects and characteristic modes in the modeling and simulation of submicron devices. *IEEE Trans. Computer-Aided Design of Integrated Circuits and Systems*, **14**:917–923, 1995.

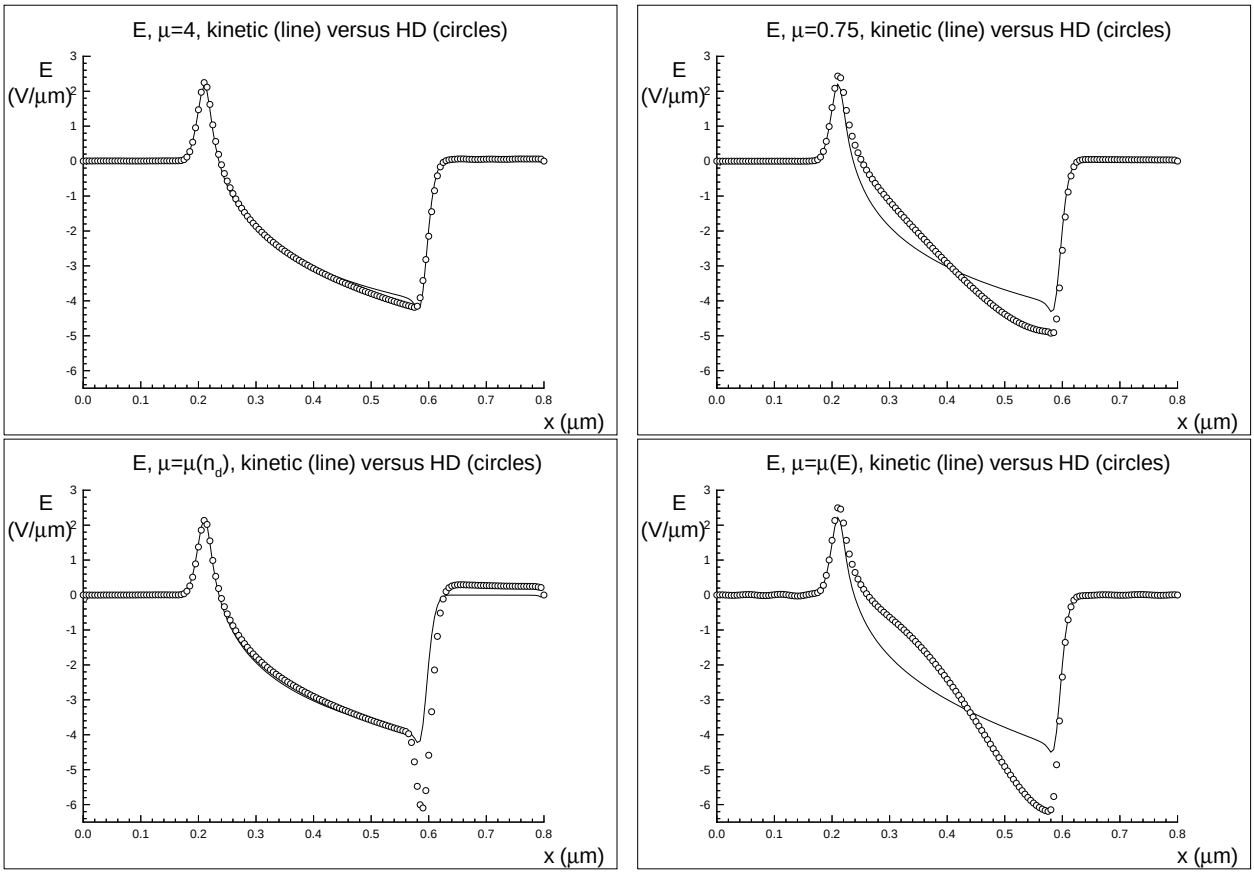

Figure 5.6: Hydrodynamic (HD) results (circles) versus kinetic simulation results (solid line), $vbias = 1$ volt. The electric field E in $volts/\mu m$. Top left: $\mu = 4$; top right: $\mu = 0.75$; bottom left: $\mu = \mu(n_d)$ as given by (2.10); bottom right: $\mu = \mu(E)$ as given by (2.11).

[10] G. Jiang and C.-W. Shu. Efficient implementation of weighted ENO schemes. *J. Comput. Phys.*, **126**:202–228, 1996.

[11] E. C. Kan, U. Ravaioli and T. Kerkhoven. Calculation of velocity overshoot in submicron devices using an augmented drift-diffusion model. *Solid-State Electr.*, **34**:995–999, 1991.

[12] C.-W. Shu and S. Osher, Efficient implementation of essentially non-oscillatory shock capturing schemes II, *J. Comput. Phys.*, **83**:32–78, 1989.

[13] K. K. Thornber. Current equations for velocity overshoot. *IEEE Electron Device Lett.*, **3**:69–71, 1983.

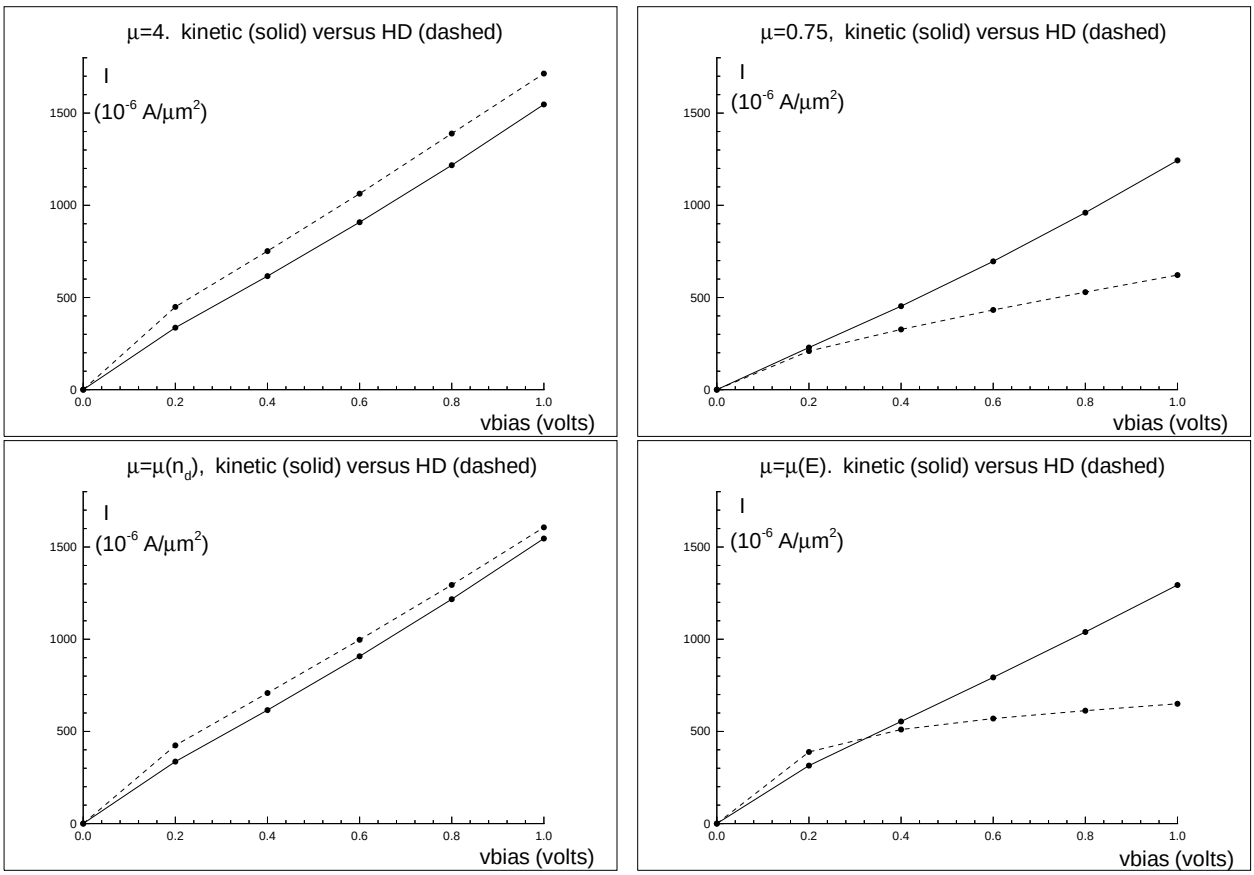

Figure 5.7: Hydrodynamic (HD) results (dashed line) versus kinetic simulation results (solid line). The I-V curve in $10^{-6} Amps/\mu m^2$ versus $volts$. Top left: $\mu = 4$; top right: $\mu = 0.75$; bottom left: $\mu = \mu(n_d)$ as given by (2.10); bottom right: $\mu = \mu(E)$ as given by (2.11).

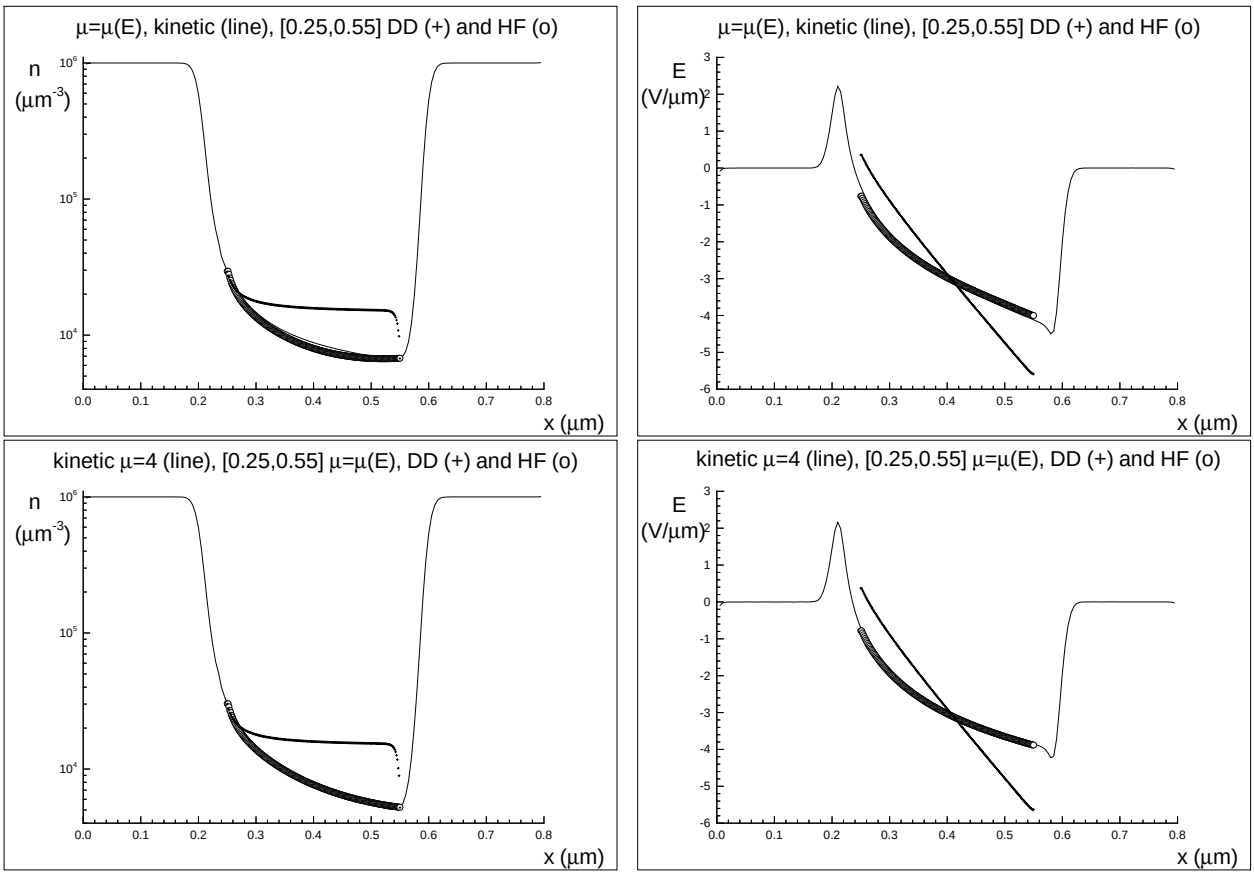

Figure 5.8: The global kinetic simulation (solid line), the mid-region HF simulation (circles), and the mid-region DD simulation (plus signs). Top: $\mu = \mu(E)$ for all simulations; bottom: $\mu = 4$ for the global kinetic simulation, which also provides the boundary conditions for the mid-region HF and DD simulations, but the HF and DD simulations use $\mu = \mu(E)$. Left: the concentration n in μm^{-3}; right: the electric field E in $volts/\mu m$.

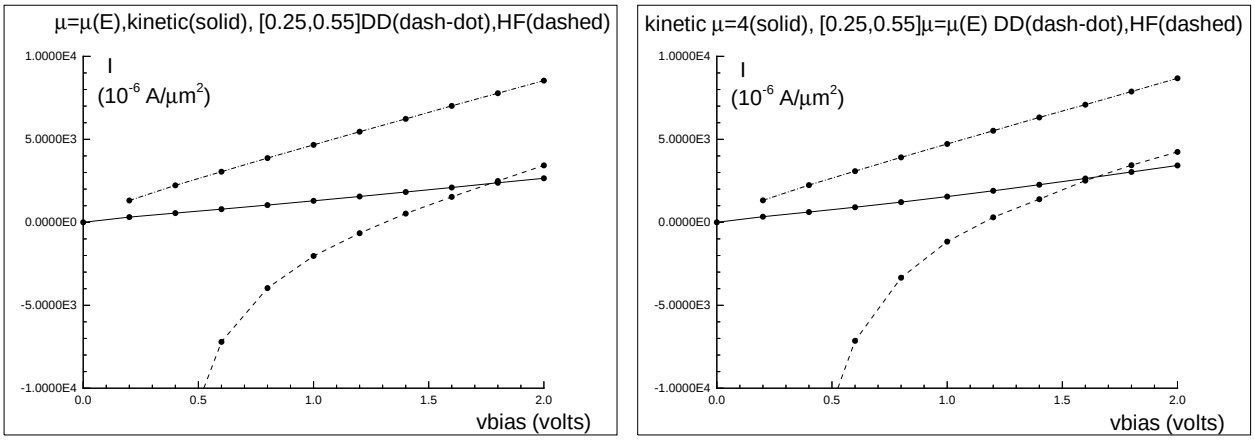

Figure 5.9: The I-V curve in $10^{-6} Amps/\mu m^2$ versus $volts$. The global kinetic simulation (solid line), the mid-region HF simulation (dashed line), and the mid-region DD simulation (dash-dots). Left: $\mu = \mu(E)$ for all simulations; right: $\mu = 4$ for the global kinetic simulation, which also provides the boundary conditions for the mid-region HF and DD simulations, but the HF and DD simulations use $\mu = \mu(E)$.